Dalton Transactions

ROYAL SOCIETY OF CHEMISTRY

PAPER

View Article Online
View Journal

Cite this: DOI: 10.1039/d5dt01508a

Crystal engineering of dinitropyrazine-based sodium E-MOFs: toward thermally robust and low-sensitivity energetic materials

Manojkumar Jujam, † Abhishek Kumar Yadav † and Srinivas Dharavath *

The strategic development of thermally stable and low-sensitivity energetic materials is vital for next-generation defence and aerospace applications. Herein, we report the synthesis of novel three-dimensional energetic metal–organic frameworks (E-MOFs), **NaNODP**, **NaNPO**, and **MDPO**, *via* a straightforward synthetic approach. The E-MOFs were confirmed by SCXRD and thoroughly characterized using PXRD, NMR, IR, TGA-DSC, and elemental analysis (EA). **NaNODP** and **NaNPO** demonstrate good detonation performance (VOD: 8100–7960 m s^{-1}; DP: 22.13–22.47 GPa), high thermal stability (T_d = 291–271 °C), and mechanical insensitivity (IS: >40 J; FS: >360 N), rendering them promising candidates for heat-resistant explosive applications exceeding **TNT** and **HNS** and comparable to **TATB**. Hirshfeld surface and 2D fingerprint analyses underscore the dominance of H···O and H···N contacts, which play a pivotal role in enhancing thermal stability and reducing mechanical sensitivity. This work offers a molecular-level approach for tuning energetic behaviour through crystal engineering and exploiting intermolecular interactions.

Received 26th June 2025,
Accepted 30th July 2025

DOI: 10.1039/d5dt01508a

rsc.li/dalton

Introduction

Heat-resistant explosives are an advanced class of energetic materials with a decomposition temperature higher than 250 °C, making them essential for heat-resistant applications such as underground blasting, space exploration, and oil drilling.[1–3] With the continuous advancement of modern society and the increasing pursuit of space and natural resource exploration, there is a growing need for high-performance, heat-resistant explosives.[4] To meet these emerging challenges, it is essential to develop new explosives that exhibit: (1) outstanding thermal stability; (2) balanced sensitivity for safe handling, transport, and initiation; (3) superior detonation capabilities; (4) reliable long-term storage properties; and (5) efficient and practical synthetic routes.[3,5] As shown in Fig. 1a, 2,2,4,4,6,6-hexanitrostilbene (**HNS**, T_d: 318 °C),[6] triaminotrinitrobenzene (**TATB**, T_d: 360 °C),[7] 2,6-bis(picrylamino)-3,5-dinitropyridine (PYX),[6,8] and 5,5′-bis(2,4,6-trinitrophenyl)-2,2′-bi(1,3,4-oxadiazole) (TKX-55)[9] are the commonly used heat-resistant explosives in real-time applications. These explosives demonstrate good thermal stability with a decomposition temperature greater than 300 °C. Although **HNS** exhibits superior thermal stability, it suffers from a relatively low detonation velocity and high sensitivity. In contrast, the thermal resistance of **TATB** is hampered by its low energy density and higher initiation threshold.[7] PYX and TKX-55 have excellent decomposition temperatures, but their practical applications are hindered by their own low nitrogen and oxygen content, and low heat of formation, which results in low detonation performance around 7700–8000 m s^{-1} and high sensitivity (5–10 J). Despite significant advancements, many heat-resistant explosives continue to suffer from limited energetic performance, environmental toxicity, and intricate synthetic procedures. As a result, there is an increasing research emphasis on the development of environmentally benign heat-resistant explosives that offer an optimal balance of energy efficiency, safety, and synthetic simplicity.[10–12]

The advancement of modern energetic materials is accelerating, as evidenced by the increasing development of energetic crystals through diverse methodologies. This embraces nitrogen-rich fused compounds and associated cocrystals, metal–organic frameworks (MOFs), binary salts, ionic liquids, and perovskite energetic substances.[13–16] MOFs, composed of metal ions or clusters coordinated with electron-donating ligands, have been praised for diverse applications such as gas storage and sensing. In recent years, MOFs have been recognized as potential high-energy density materials (HEDMs) owing to their intrinsic properties of high thermal stability, elevated mechanical sensitivity, and high heat of

Energetic Materials Laboratory, Department of Chemistry, Indian Institute of Technology Kanpur, Kanpur-208016, Uttar Pradesh, India.
E-mail: srinivasd@iitk.ac.in
† These authors contributed equally.

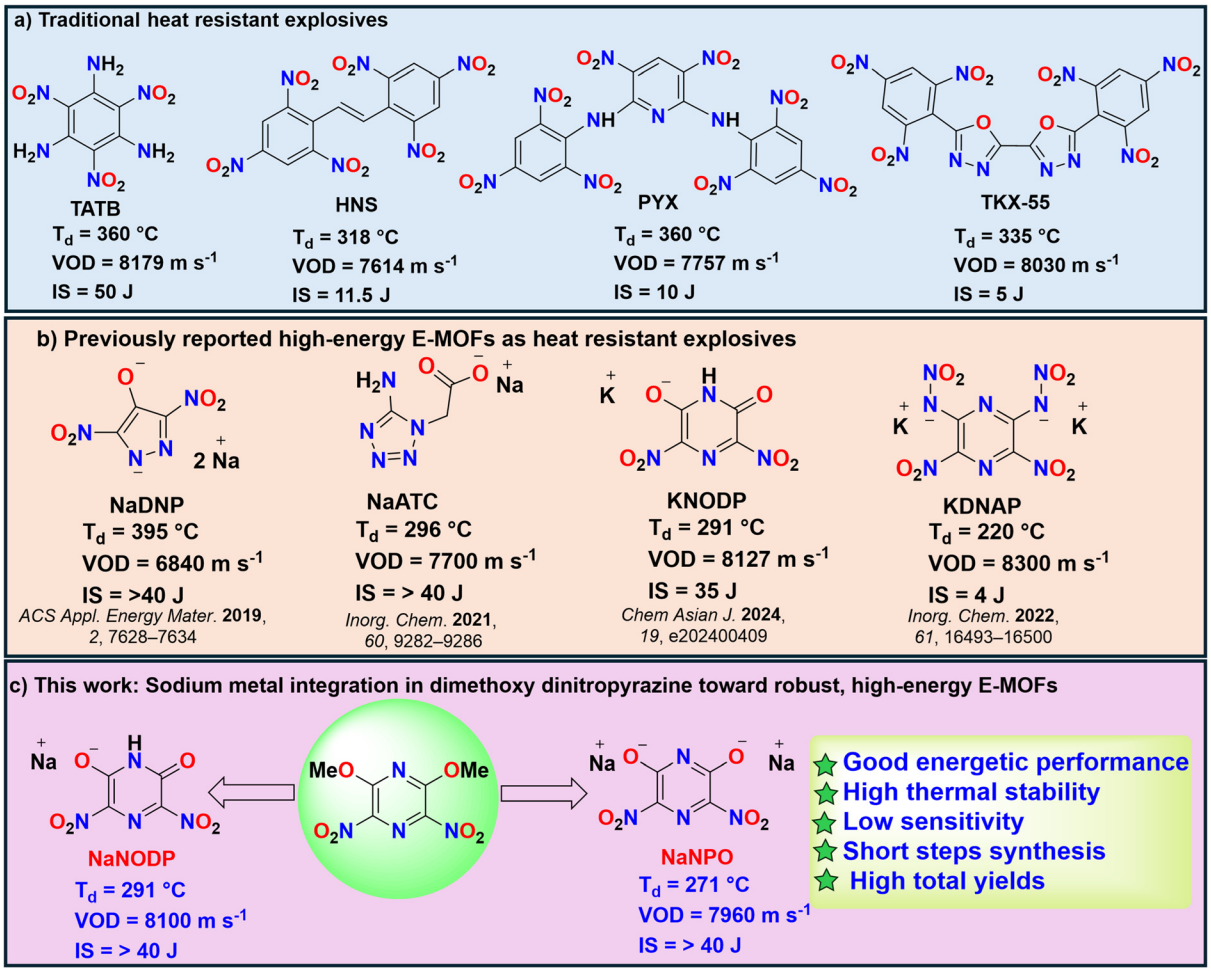

Fig. 1 Previous reports and this work demonstrate sodium-based energetic metal–organic frameworks as heat-resistant explosives.

detonation.[17,18] Since 1990, around 20 000 MOFs have been reported. Compared to many other materials used across different fields, energetic MOFs remain relatively novel, with only a limited number synthesized and energetically characterized for their potential as energetic materials. For the first time, in 2013, Pang *et al.* published two 3D high-energy metal–organic frameworks with Cu and Ag metals, which demonstrated high thermal stability associated with high heat of detonation in contrast to 1D and 2D structures.[19] While transition-metal-based E-MOFs have shown promising energetic performance, researchers have increasingly turned their attention to alkali-metal-based E-MOFs to further improve safety and environmental sustainability. Alkali-metal-based E-MOFs generally form more coordination bonds with organic ligands than their transition-metal counterparts, resulting in enhanced thermal stability.[20,21] Among them, sodium stands out as a preferable metal centre due to its environmentally friendly nature, minimizing pollution both during and after detonation.

The literature shows that very few EMOFs have achieved a fine balance between energy and stability.[22–24] In 2019, disodium 3,5-dinitro-4-hydropyrazolate (**NaDNP**) was reported as a potentially heat-resistant explosive with a decomposition temperature of 395 °C.[21] Another sodium-based EMOF, $[Na(atza)]_n$ (**NaATC**), exhibits high thermal stability at 296 °C. However, their applications are limited due to their low detonation velocities of 6840 and 7700 m s^{-1}, as shown in Fig. 1b.[25] On the other hand, six-membered E-MOFs are notably scarce in the literature. Interestingly, existing reports suggest that six-membered rings tend to show better detonation performance. In 2022, potassium(3,5-dinitropyrazine-2,6-diyl)bis(nitroamide) (**KDNAP**) was reported with good energetic performance (8300 m s^{-1}) but lags behind due to its sensitivity of 4 J.[25] In 2024, our group reported the potassium E-MOF 3,5-dinitro-6-oxo-1,6-dihydropyrazin-2-olate (**KNODP**), balancing both energy and stability with a detonation velocity of 8127 s^{-1} and good thermal stability of 291 °C.[21] This highlights the need for the development of high-performing and heat-resistant explosives. In 2023, our group reported a polytetrazole heat-resistant sodium EMOF $[Na_3(TTzTA)_3(H_2O)_6]_n$ with a decomposition temperature of 344 °C and a detonation velocity of 8500 m s^{-1}.[26] The performance and stability of energetic MOFs mostly depend on the energetic ligand.[27–29] Heterocyclic nitrogen-rich energetic ligands have been widely employed in the develop-

ment of potential EMOFs due to their favourable energetic and structural properties. In particular, heterocycles such as pyrazole, triazole, tetrazole, oxadiazole, pyrimidine, pyrazine, and triazine are of significant interest, as they serve as key building blocks in the design of novel energetic materials owing to their high density, excellent thermal stability, favourable detonation performance, and low sensitivity to external stimuli.[30]

By keeping all these in mind, we have designed and synthesized the following EMOFs: disodium 3,5-dinitropyrazine-2,6-bis(olate) (**NaNPO**), sodium 3,5-dinitro-6-oxo-1,6-dihydropyrazin-2-olate (**NaNODP**), and 6-methoxy-3,5-dinitropyrazin-2-olate (**MDPO**). Single-crystal X-ray diffraction (SCXRD) analysis confirms that **NaNPO**, **NaNODP**, and **MDPO** form three-dimensional (3D) framework architectures. The comprehensive characterization of the synthesized EMOFs was carried out using PXRD, IR, elemental analysis, NMR spectroscopy, and DSC measurements. Given their outstanding thermal stability, good energetic performance, and insensitivity, **NaNPO** and **NaNODP** are strong candidates for use as heat-resistant explosives.

Synthesis

The energetic ligand 2,6-dimethoxy-3,5-dinitropyrazine (**1**) and trisodium 3,5-bis(nitroimino)-1,2,4-triazolidine-1,2,4-tride (Na-MOF) were synthesized based on the previous literature.[20,31] Ligand **1** and Na-MOF were heated in a 1 : 1 ratio of acetonitrile and water at 90 °C for 15 hours, resulting in **NaNODP** with a yield of 70%. Further treatment of ligand **1** with two equivalents of aqueous sodium carbonate at 100 °C for 15 hours *via* a hydrothermal process produced red-colored crystals of **NaNPO** with 75% yield. **MDPO** was isolated by refluxing ligand **1** with one equivalent of aqueous sodium hydroxide, giving yellow crystals with 60% yield (Scheme 1).

Crystal description

High-quality single crystals of **NaNODP** were successfully grown *via* slow evaporation of a mixed solvent system comprising acetonitrile and water at ambient temperature. The compound crystallized in the triclinic crystal system with the space group $P\bar{1}$, exhibiting a crystal density of 1.93 g cm^{-3} at 100 K. The asymmetric unit comprises the energetic ligand and one sodium metal ion. Additionally, a second sodium metal ion, excluded from the formal molecular formula, is linked *via* a bridging water molecule, resulting in a coordination bridge between the two sodium centres and contributing to the extended supramolecular framework, as shown in Fig. 2a. Fig. 2b illustrates the coordination nature of the energetic ligand with sodium. Each Na(I) is coordinated with two oxygen atoms from the energetic ligand and four oxygen atoms from the coordinated water molecules. The observed Na–O coordination bond lengths, ranging from 2.31 to 2.40 Å, contribute to forming stable three-dimensional frameworks. Fig. 2(c and d) show the layered packing structure of **NaNODP** along the *a* and *b*-axis.

Red-coloured crystals of **NaNPO** were obtained directly from the reaction vessels upon cooling to ambient temperature. The asymmetric unit consists of an energetic ligand, two independent sodium ions (Na1(I) and Na2(I)), and two coordinated water molecules. **NaNPO** crystallized in the triclinic crystal system with the space group $P\bar{1}$, exhibiting a crystal density of 2.09 g cm^{-3} at 100 K. As illustrated in Fig. 3b, Na1(I) adopts an

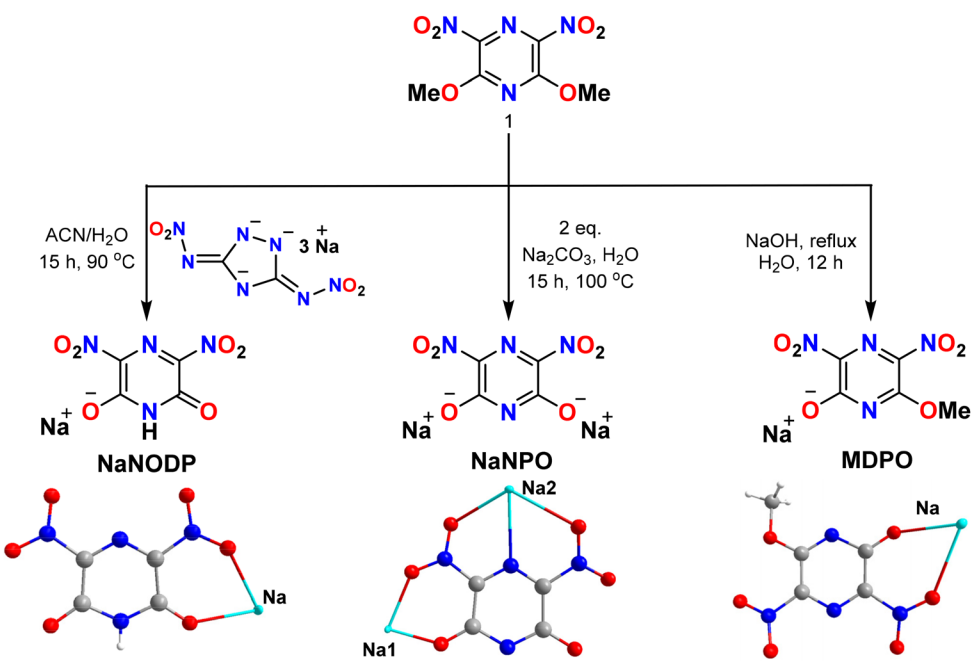

Scheme 1 Hydrothermal synthesis of energetic metal–organic frameworks.

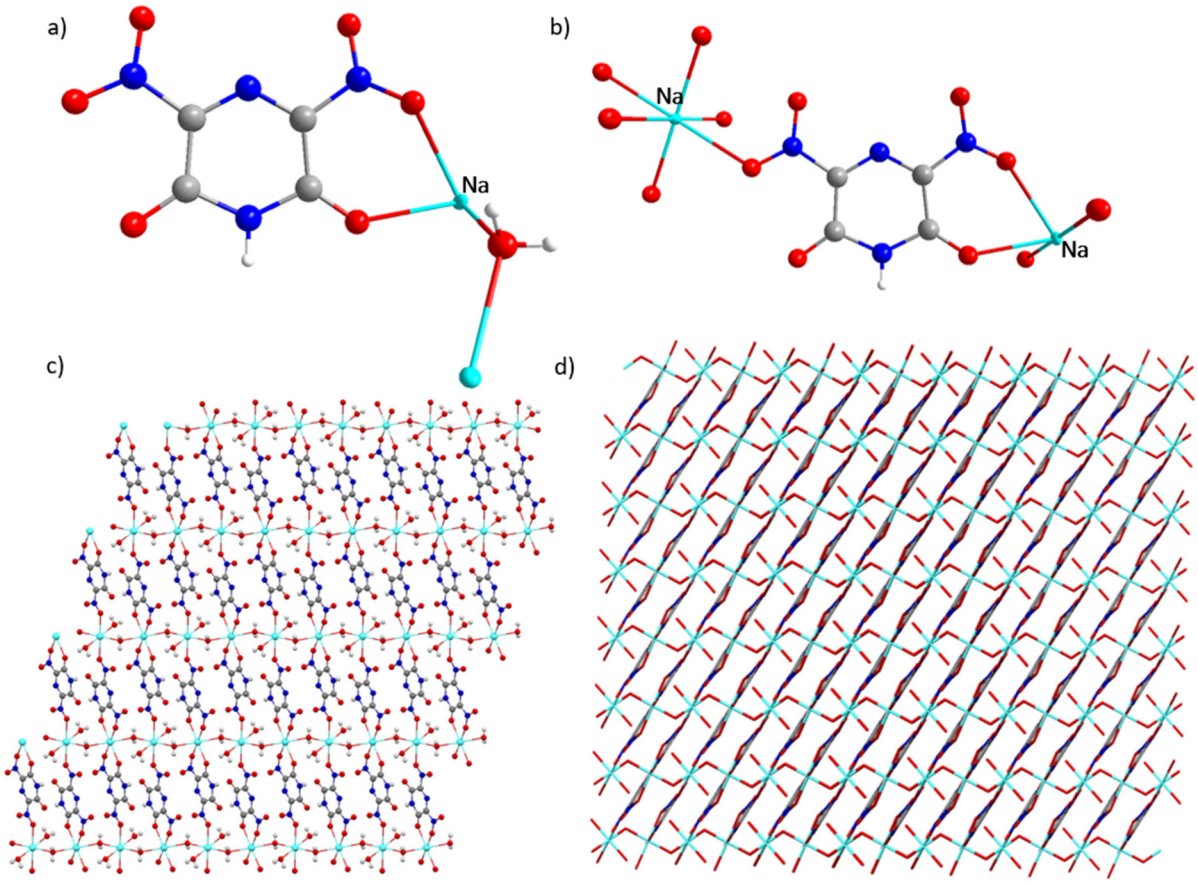

Fig. 2 (a) Asymmetric unit of **NaNODP**. (b) The coordination environment of the ligand with Na(I) ions and the coordination environment of Na(I). (c and d) Enlarged view of the porous crystal packing diagram of **NaNODP** along the *a*-axis and *b*-axis.

octacoordinated geometry, interacting with six oxygen atoms from the ligand and two from coordinated water molecules. Na2 (I), on the other hand, exhibits an N_1O_6 coordination environment, involving one nitrogen and three oxygen atoms from the ligand and three oxygen atoms from coordinated water molecules. Each ligand coordinates with six adjacent Na(I) ions within the crystal framework, as shown in Fig. 3c. As shown in Fig. 3d, **NaNPO** exhibits a porous three-dimensional crystal packing along the *a*-axis. The energetic ligand acquires the planar configuration and two independent sodium ions lying above and below the plane, as shown in Fig. 3e. Fig. 3f replicates the packing diagram of **NaNPO**, showing a wave-like pattern resembling the structure of DNA, where water molecules act as bridges similar to the hydrogen bonds that stabilize DNA strands.

Yellow-coloured crystals of **MDPO** were obtained *via* slow evaporation of the reaction mixture at room temperature. The compound crystallized in the monoclinic system with the space group $P2_1/n$ and a crystal density of 1.86 g cm^{-3}. The asymmetric unit contains one ligand and one sodium ion, as displayed in Fig. 4a. Each ligand coordinates tetrahedrally to four Na(I) ions (Fig. 4a and b), while each sodium ion is octacoordinated in an N_2O_6 environment provided by the ligand. The **MDPO** ligand adopts an almost planar conformation, lying entirely within a single plane (Fig. 4f). The three-dimensional crystal packing along the *a* and *b* axes reveals substantial voids, indicative of a porous structure and potential utility in adsorption applications (Fig. 4(d, e and g)).

Additionally, bulk powder samples of E-MOFs were prepared using the same synthetic procedures to carry out further physicochemical and energetic property evaluations. To verify the bulk purity of the synthesized E-MOFs, powder X-ray diffraction analysis was conducted using PANalytical X'Pert. The PXRD pattern of the synthesized E-MOFs corresponds closely to the simulated XRD pattern derived from the SC-XRD data, confirming the high purity of the powder samples, as shown in Fig. S18.

Physicochemical and energetic properties

Thermal stability is a key criterion for evaluating the safety of heat-resistant explosives under extreme conditions. The thermal behaviour of anhydrous energetic compounds was investigated using differential scanning calorimetry (DSC) at a heating rate of 5 °C min^{-1} under a dry nitrogen atmosphere. E-MOFs **NaNODP** and **NaNPO** displayed high thermal stability, with decomposition temperatures of 291 °C and 271 °C, respectively, as shown in Fig. 5. Their crystal densities, determined at

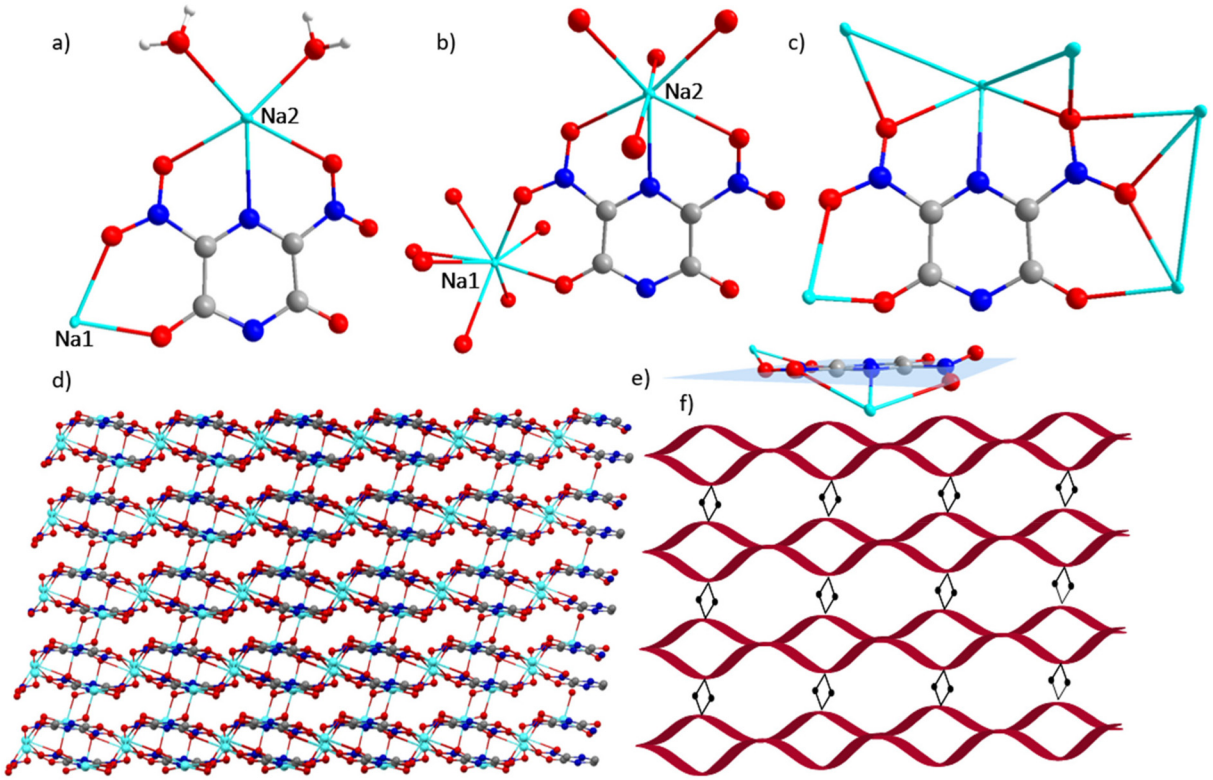

Fig. 3 (a) Asymmetric unit of **NaNPO**. (b and c) The coordination environment of Na(I). (d) The coordination environment of the ligand with Na(I) ions. (d) 3D porous crystal packing diagram of **NaNPO** along the *a*-axis. (e) Planarity of NaNPO. (f) Packing diagram of **NaNPO**, showing a wave-like pattern resembling the structure of DNA.

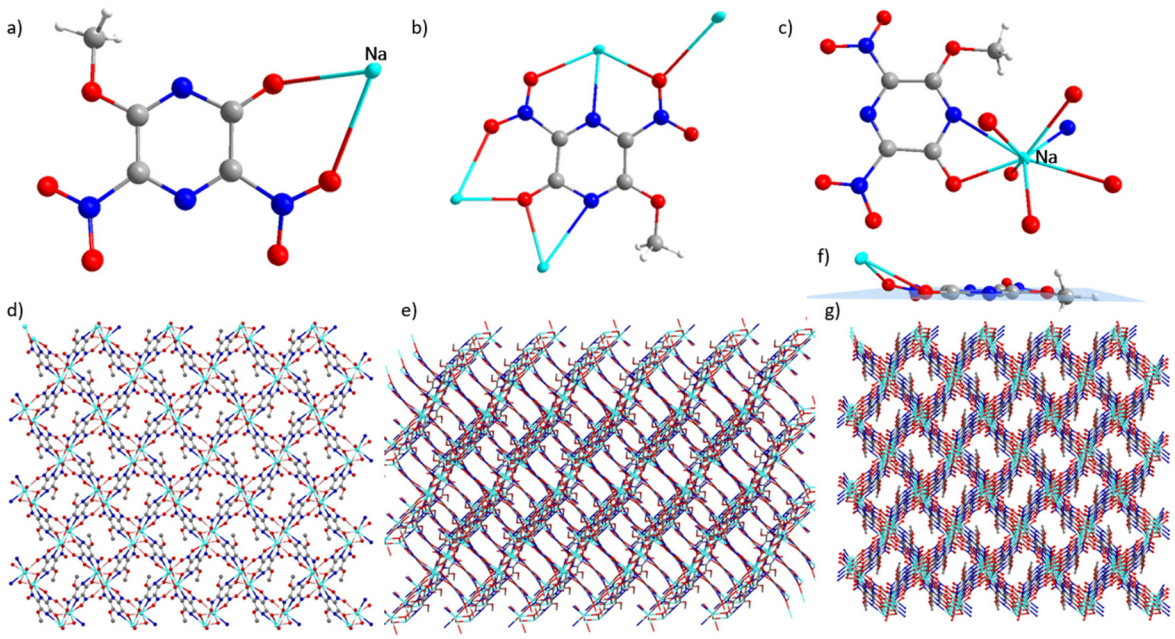

Fig. 4 (a) Asymmetric unit of **MDPO**. (b) The coordination environment of the ligand with Na(I) ions. (c) The coordination environment of Na(I). (f) Planarity of **MDPO**. (d, e, and g) Enlarged view of the porous crystal packing diagram of **MDPO** along the *a*-axis and *b*-axis.

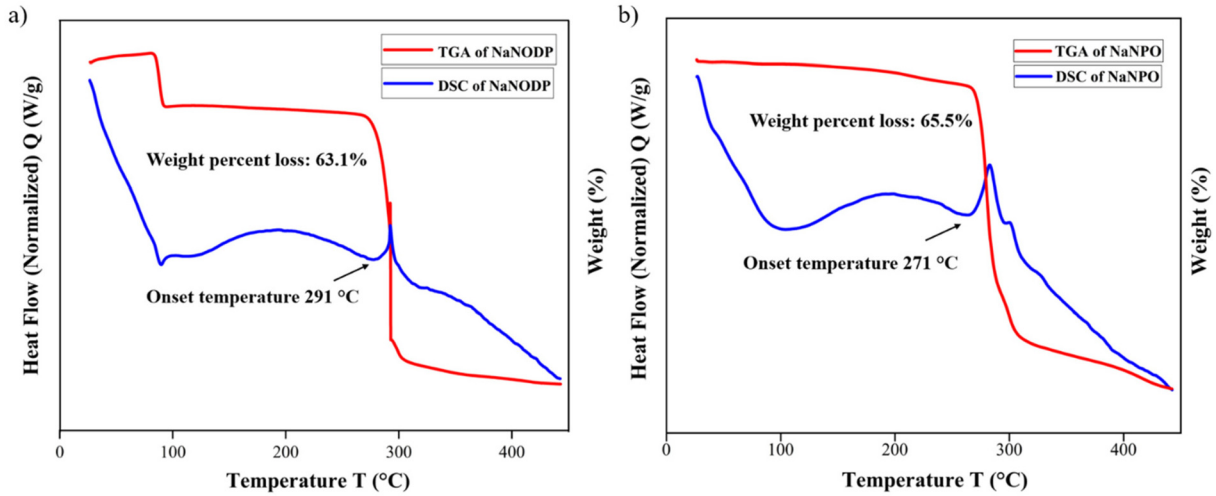

Fig. 5 (a and b) TGA-DSC graphs of **NaNODP** and **NaNPO**, respectively.

100 K, range from 1.93 to 2.09 g cm^{-3}, surpassing those of **HNS** (1.75 g cm^{-3}), **TNT** (1.65 g cm^{-3}), **TATB** (1.93 g cm^{-3}), and previously reported compounds such as NaDNAP (1.85 g cm^{-3})[21] and **NaATC** (1.82 g cm^{-3}).[25] Heats of formation (ΔH_f) were computed using Gaussian 09 and found to lie between −445.81 and −712.21 kJ mol^{-1} for **NaNODP** and **NaNPO**.

Based on the measured densities and computed heat of formation values, detonation velocities (VOD) and detonation pressures (DP) were calculated using the Explo5 v7.01.01 software. **NaNODP** exhibited a VOD of 8100 m s^{-1} and DP of 22.13 GPa, which approaches close to that of **TATB** (VOD = 8179 m s^{-1}, DP = 30.5 GPa), while **NaNPO** achieved 7960 m s^{-1} and 22.47 GPa, surpassing **TNT** (VOD = 6881 m s^{-1}, DP = 19.5 GPa) and the benchmark heat resistant explosive, namely **HNS** (VOD = 7164 m s^{-1}, DP = 21.6 GPa). These values also surpass those of the previously reported **NaDNP** and **NaATC** and are close to that of NaTT as listed in Table 1. Mechanical sensitivities were evaluated using a BAM fall hammer and friction tester. The E-MOFs demonstrated low impact sensitivity (>40 J) and high friction resistance (>360 N), in contrast to **HNS** (IS: 11.5 J, FS: 240 N),[6,33] which is attributed to strong coordination between metal centres and organic linkers. The combined advantages of high density, excellent energetic performance, low sensitivity, and superior thermal stability position **NaNODP** and **NaNPO** as promising candidates for next-generation heat-resistant explosives.

Hirshfeld surface

Hirshfeld surface and two-dimensional fingerprint analyses were conducted for **NaNODP**, **NaNPO**, and **MDPO** to obtain a better understanding of the intermolecular interactions in their crystal structures. The Hirshfeld surface displays red spots, indicating strong interactions between atoms where the distance is less than their van der Waals distance, while blue and white spots indicate weaker interactions. Fig. 6a illustrates the Hirshfeld surfaces of **NaNODP**, **NaNPO**, and **MDPO**, revealing almost planar configurations. The pronounced red spots observed across the surfaces predominantly arise from strong intermolecular hydrogen-bonding interactions, notably H···O/O···H and H···N/N···H contacts, which play a crucial role in stabilizing the crystal packing.

Table 1 Physicochemical and energetic properties of EMOFs

Compounds	T_d [a] [°C]	ρ [b] [g cm^{-3}]	HOF[c] [kJ mol^{-1}]	VOD[d] [m s^{-1}]	DP[e] [GPa]	IS[f] [J]	FS[g] [N]	N + O[h] [%]
NaNODP	291	1.93	−445.8	8100	22.13	>40	>360	67.8
NaNPO	271	2.09	−712.2	7960	22.47	>40	>360	61.7
NaDNP [21]	395	2.13[i]	−445	6840	20.98	>40	>360	62.3
KNODP [21]	291	2.16	−535.5	8127	26.94	35	360	63.3
KDNAP [25]	220	2.10[i]	−106.7	8300	29.9	4	40	65.5
NaATC [25]	296	1.82	612.5[j]	7700	26.53	>40	>360	61.8
TNT [32,33]	295	1.65	−67	6881	19.5	39.2	353	60.7
HNS [6,33]	318	1.75	78.2	7164	21.6	11.5	240	61.3
TATB [7,33]	360	1.93	137.5	8179	30.5	112	>360	69.7

[a] Onset decomposition temperature (5 °C min^{-1}). [b] Crystal density. [c] Computed HOF. [d] Detonation velocity. [e] Detonation pressure. [f] Impact sensitivity. [g] Friction sensitivity. [h] Nitrogen and oxygen percentages. [i] Density, gas pycnometer at 25 °C. [j] HOF from the bomb calorimeter.

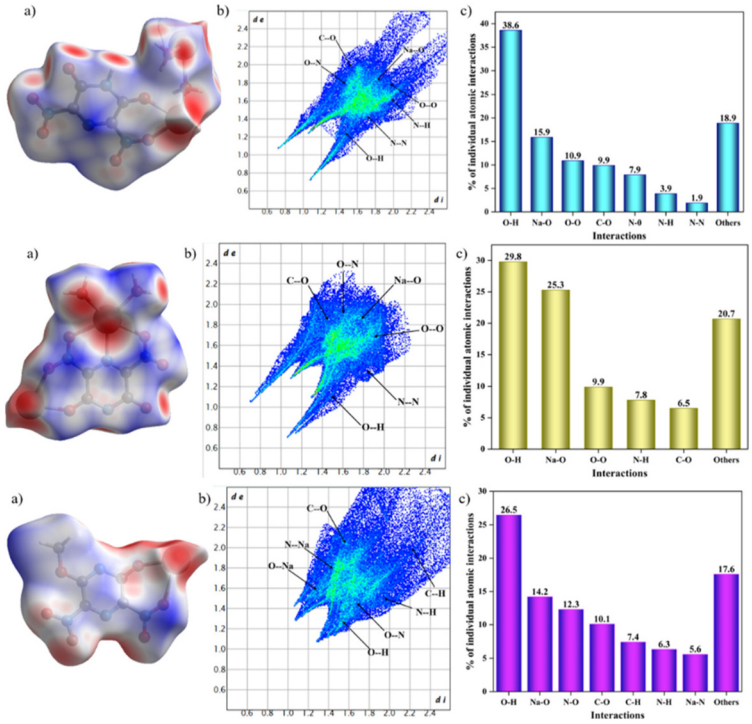

Fig. 6 (a) Hirshfeld surfaces of **NaNODP**, **NaNPO**, and **MDPO**; (b) two-dimensional fingerprint plots of **NaNODP**, **NaNPO**, and **MDPO**; and (c) individual atomic contributions corresponding to the 2D fingerprint plots.

As shown in Fig. 6b, the 2D fingerprint plots exhibit two sharp spikes, corresponding to hydrogen bonding (HB) interactions. The percentage contributions of HBs (N···H and O···H) were 37.6%, 42.5%, and 32.8% for **NaNODP**, **NaNPO**, and **MDPO**, respectively, suggesting that hydrogen bonding stabilizes the energetic frameworks and enhances thermal stability and insensitivity, as shown in Fig. 6c. **NaNPO** has 25.3% of Na···O strong coordinated interactions compared to **NaNODP** and **MDPO**, which show 15.9% and 14.2%, respectively, also contributing to the stability of the frameworks. The coplanar conjugated frameworks of **NaNODP**, **NaNPO**, and **MDPO** promote a layer-by-layer molecular arrangement within their crystal lattices. These non-covalent interactions, including N···N, C···N, and N···O contacts, were consistently observed across all three crystal structures, with corresponding average contributions of 19.7%, 6.5%, and 22.4%, respectively. The presence of these non-covalent interactions plays a vital role in reinforcing crystal stability by enhancing intermolecular attractions, which may also contribute to reduced mechanical sensitivity, such as impact or friction.

Conclusion

In conclusion, we have designed and synthesized novel 3D E-MOFs through a facile synthetic approach. All E-MOFs were confirmed by SCXRD and thoroughly characterized using PXRD, NMR, IR, TGA-DSC, and elemental analysis. The crystal structures of **NaNODP** and **NaNPO** reveal extensive intermolecular hydrogen-bonding interactions, which contribute to enhanced thermal stability and reduced sensitivity. **NaNODP** and **NaNPO** exhibit promising detonation performance (VOD = 8100–7960 m s^{-1}; DP = 22.13–22.47 GPa), superior thermal stability (T_d = 291–271 °C), and mechanical insensitivity (IS = >40 J; FS = >360 N). Among them, **NaNPO** stands out due to its excellent thermal stability, high density (2.09 g cm^{-3}), and favourable detonation performance (VOD = 7960 m s^{-1}, DP = 22.47 GPa), making it a potential candidate for heat-resistant explosives, comparable to **HNS** (VOD = 7164 m s^{-1}, DP = 21.6 GPa, T_d = 318 °C). **NaNODP**, on the other hand, demonstrates good density (1.93 g cm^{-3}) and good detonation velocity (VOD = 8100 m s^{-1}, DP = 22.13 GPa), approaching that of the traditional secondary explosive **TATB** (VOD = 8179 m s^{-1}, DP = 30.5 GPa). These findings offer a promising strategy for the development of balanced heat-resistant explosives with the distinct advantages of MOF architectures for practical applications.

Caution! All the compounds investigated are potentially explosive, energetic materials. Although we have experienced no difficulties in the synthesis and characterization of these compounds, manipulations must be carried out by using appropriate standard safety precautions. Eye protection and leather gloves must always be worn.

Author contributions

Manojkumar Jujam: conceptualization; methodology; investigation; validation; formal analysis; and writing – original

draft. Abhishek Kumar Yadav: conceptualization; methodology; investigation; validation; formal analysis; and writing – original draft. Srinivas Dharavath: conceptualization; methodology; validation; supervision; funding acquisition; software; project administration; writing – original draft; writing – review & editing. The manuscript was written through the contributions of all authors. All authors have approved the final version of the manuscript.

Conflicts of interest

The authors declare no competing financial interest.

Data availability

The data underlying this study are available in the published article and its SI: synthesis, characterization data, computational details, crystal refinements, X-ray crystallographic file in CIF format for **NaNODP**, **NaNPO** and **MDPO**. See DOI: **https://doi.org/10.1039/d5dt01508a**.

CCDC 2457669–2457671 contain the supplementary crystallographic data for this paper.[34a–c]

Acknowledgements

MJ thanks PMRF for the fellowship, and AKY thanks IIT Kanpur for the FARE fellowship. MJ and AKY thank IIT Kanpur for the infrastructure. SD is grateful for the financial support from the CRG scheme (no. CRG/2023/000007), Science and Engineering Research Board, Department of Science and Technology, Government of India.

References

1 R. Zhang, Y. Xu, F. Yang, P. Wang, Q. Lin, H. Huang and M. Lu, *Def. Technol.*, 2024, **38**, 33–57.
2 T. Yan, H. Yang, C. Yang, Z. Yi, S. Zhu and G. Cheng, *J. Mater. Chem. A*, 2020, **8**, 23857–23865.
3 C. Li, T. Zhu, J. Tang, G. Cheng, C. Xiao and H. Yang, *J. Org. Chem.*, 2025, **90**, 4505–4512.
4 B. Tan, J. Dou, X. Yang, W. Li, J. Zhang, P. Zhang, H. Mo, X. Lu, B. Wang and N. Liu, *Dalton Trans.*, 2024, **53**, 13308–13319.
5 Z. Xu, C. Lei, Q. Wang, J. Tang, G. Cheng and H. Yang, *Cryst. Growth Des.*, 2023, **23**, 8197–8203.
6 M. Jujam, V. D. Ghule and S. Dharavath, *J. Org. Chem.*, 2024, **89**, 8192–8200.
7 Y. Wang, Y. Liu, Y. Liu, S. Song, Z. Yang, X. Qi, K. Wang, Q. Zhang and Y. Tian, *Nat. Commun.*, 2018, **9**, 2444.
8 N. Liu, Q. Zhang, B. Duan, X. Lu, X. Bai and Q. Yan, *FirePhysChem*, 2021, **1**, 61–69.
9 T. M. Klapötke and T. G. Witkowski, *ChemPlusChem*, 2016, **81**, 357–360.
10 A. K. Yadav, V. D. Ghule and S. Dharavath, *ACS Appl. Mater. Interfaces*, 2022, **14**, 49908.
11 T. G. Witkowski, E. Sebastiao, B. Gabidullin, A. Hu, F. Zhang and M. Murugesu, *ACS Appl. Energy Mater.*, 2018, **1**, 589–593.
12 Y. Tang, C. He, G. H. Imler, D. A. Parrish and J. M. Shreeve, *ACS Appl. Energy. Mater.*, 2019, **2**, 2263–2267.
13 Y. Feng, S. Chen, M. Deng, T. Zhang and Q. Zhang, *Inorg. Chem.*, 2019, **58**, 12228–12233.
14 S. Banik, V. D. Ghule and S. Dharavath, *J. Mater. Chem. A*, 2025, **13**, 11286–11292.
15 Q. Zhang and J. M. Shreeve, *Chem. Rev.*, 2014, **114**, 10527–10574.
16 S. Chen, Z. Yi, C. Jia, Y. Li, H. Chen, S. Zhu and L. Zhang, *Small*, 2023, **19**, 2302631.
17 Y. Tang, C. He, L. A. Mitchell, D. A. Parrish and J. M. Shreeve, *Angew. Chem., Int. Ed.*, 2016, **55**, 5565–5567.
18 S. Zhang, Q. Yang, X. Liu, X. Qu, Q. Wei, G. Xie, S. Chen and S. Gao, *Coord. Chem. Rev.*, 2016, **307**, 292–312.
19 S. Li, Y. Wang, C. Qi, X. Zhao, J. Zhang, S. Zhang, S. Pang, S. Li, Y. Wang, C. Qi, X. Zhao, J. Zhang, S. Pang and S. Zhang, *Angew. Chem., Int. Ed.*, 2013, **52**, 14031–14035.
20 M. Jujam, R. Rajak and S. Dharavath, *Adv. Funct. Mater.*, 2025, **35**, 2412638.
21 (*a*) J. Zhang, J. Zhang, G. H. Imler, D. A. Parrish and J. M. Shreeve, *ACS Appl. Energy Mater.*, 2019, **2**, 7628–7634; (*b*) A. K. Yadav, V. D. Ghule and S. Dharavath, *Chem. – Asian J.*, 2024, **19**, e202400409.
22 R. Rajak, N. Kumar, V. D. Ghule and S. Dharavath, *ACS Appl. Mater. Interfaces*, 2024, **16**, 20670–20680.
23 P. He, J. G. Zhang, L. Wu, J. T. Wu and T. L. Zhang, *Inorg. Chim. Acta*, 2017, **455**, 152–157.
24 D. Chen, D. Jing, Q. Zhang, X. Xue, S. Gou, H. Li and F. Nie, *Chem. – Asian J.*, 2017, **12**, 3141–3149.
25 (*a*) C. Liang, J. Yang, Y. Guo, F. Yuan, W. Song, J. Xi, X. Liu and S. Chen, *Inorg. Chem.*, 2021, **60**, 9282–9286; (*b*) J. Singh, A. K. Chinnam, R. J. Staples and J. M. Shreeve, *Inorg. Chem.*, 2022, **61**, 16493–16500.
26 R. Rajak, P. Kumar, V. D. Ghule and S. Dharavath, *Inorg. Chem.*, 2023, **62**, 8389–8396.
27 T. Yan, J. Ma, H. Yang and G. Cheng, *Chem. Eng. J.*, 2022, **429**, 132416.
28 Q. Ma, G. Zhang, J. Li, Z. Zhang, H. Lu, L. Liao, G. Fan and F. Nie, *Chem. Eng. J.*, 2020, **379**, 122331.
29 S. Nehe, A. K. Yadav, V. D. Ghule and S. Dharavath, *Org. Lett.*, 2025, **27**, 5169.
30 P. Kumar, V. D. Ghule and S. Dharavath, *Org. Lett.*, 2022, **24**, 3555–3559.
31 P. Pagoria, M. X. Zhang, N. Zuckerman, G. Lee, A. Mitchell, A. DeHope, A. Gash, C. Coon and P. Gallagher, *Propellants, Explos., Pyrotech.*, 2018, **43**, 15–27.
32 Z. Xu, G. Cheng, S. Zhu, Q. Lin and H. Yang, *J. Mater. Chem. A*, 2018, **6**, 2239–2248.
33 (*a*) S. Zeman and V. B. Patil, *FirePhysChem*, 2025, **5**, 68–73; (*b*) *Chem. Phys. Energy Mater*, ed. C. B. Storm, J. R. Stine,

J. F. Kramer and S. N. Bulusu, Kluwer Acad. Publ., Dordrecht, 1990, pp. 605–639.

34 (*a*) M. Jujam, A. K. Yadav and S. Dharavath, CCDC 2457669: Experimental Crystal Structure Determination, 2025, DOI: **10.5517/ccdc.csd.cc2nhdn7**; (*b*) M. Jujam, A. K. Yadav and S. Dharavath, CCDC 2457670: Experimental Crystal Structure Determination, 2025, DOI: **10.5517/ccdc.csd.cc2nhdp8**; (*c*) M. Jujam, A. K. Yadav and S. Dharavath, CCDC 2457671: Experimental Crystal Structure Determination, 2025, DOI: **10.5517/ccdc.csd.cc2nhdq9**.